Pathogen manipulation of chloroplast function triggers a light-dependent immune recognition

Chuyun Gao[a], Huawei Xu[a], Jie Huang[a], Biying Sun[a], Fan Zhang[a], Zachary Savage[b], Cian Duggan[b], Tingxiu Yan[a], Chih-hang Wu[c], Yuanchao Wang[a,d], Vivianne G. A. A. Vleeshouwers[e], Sophien Kamoun[c], Tolga O. Bozkurt[b], and Suomeng Dong[a,c,d,1]

[a]College of Plant Protection, Nanjing Agricultural University, 210095 Nanjing, China; [b]Imperial College, South Kensington Campus, SW7 2AZ London, United Kingdom; [c]The Sainsbury Laboratory, University of East Anglia, NR4 7UH Norwich, United Kingdom; [d]Key Laboratory of Plant Immunity, Nanjing Agricultural University, 210095 Nanjing, China; and [e]Wageningen University and Research Plant Breeding, Wageningen University and Research, Wageningen 6708 PB, The Netherlands

In plants and animals, nucleotide-binding leucine-rich repeat (NLR) proteins are intracellular immune sensors that recognize and eliminate a wide range of invading pathogens. NLR-mediated immunity is known to be modulated by environmental factors. However, how pathogen recognition by NLRs is influenced by environmental factors such as light remains unclear. Here, we show that the agronomically important NLR Rpi-vnt1.1 requires light to confer disease resistance against races of the Irish potato famine pathogen *Phytophthora infestans* that secrete the effector protein AVRvnt1. The activation of Rpi-vnt1.1 requires a nuclear-encoded chloroplast protein, glycerate 3-kinase (GLYK), implicated in energy production. The pathogen effector AVRvnt1 binds the full-length chloroplast-targeted GLYK isoform leading to activation of Rpi-vnt1.1. In the dark, Rpi-vnt1.1–mediated resistance is compromised because plants produce a shorter GLYK—lacking the intact chloroplast transit peptide—that is not bound by AVRvnt1. The transition between full-length and shorter plant GLYK transcripts is controlled by a light-dependent alternative promoter selection mechanism. In plants that lack Rpi-vnt1.1, the presence of AVRvnt1 reduces GLYK accumulation in chloroplasts counteracting GLYK contribution to basal immunity. Our findings revealed that pathogen manipulation of chloroplast functions has resulted in a light-dependent immune response.

potato blight | NLR | disease resistance | light | chloroplast

Unlike animals, plants lack adaptive immunity that recognizes and eliminates invading pathogens actively. Therefore, cell-autonomous immunity plays critical roles in plants to sense and defend pathogen infections. Recognition of pathogen-associated molecular patterns by cell pattern recognition receptors (PRRs) activates innate immune responses effectively against the invaders (1, 2). In turn, adapted pathogens secrete a mixture of effector proteins to suppress or evade immunity triggered by PRRs. Some of the host-translocated effectors are directly or indirectly recognized by highly specialized intracellular immune sensors called the nucleotide-binding leucine-rich repeat (NLR) proteins (3). Activation of NLRs triggers a robust immune response which typically involves a form of localized cell death implicated in arresting pathogen growth called the hypersensitive response (HR) (4, 5).

In potato, resistance to Irish potato famine pathogen *Phytophthora infestans* is mainly conferred by the coil–coil type of NLRs, which were mostly identified in wild *Solanum* species. One such NLR called Rpi-vnt1.1 cloned from *Solanum venturii* draws extensive attention as being the first plant disease resistance protein commercialized in a genetically modified crop (6). Rpi-vnt1.1 recognizes a host-translocated RxLR type of effector protein called AVRvnt1 that is present in all *P. infestans* strains examined so far. Although *AVRvnt1* shows sequence polymorphism in different isolates, all of the tested alleles of *AVRvnt1* are known to activate Rpi-vnt1.1–mediated resistance.

The only exception is the *P. infestans* isolate P13626, from the asexual lineage EC-1, which evades Rpi-vnt1 recognition due to the down-regulation of *AVRvnt1* gene expression (7). Interestingly, a closely related isolate P13527 from the same asexual lineage maintains normal AVRvnt1 expression and can be recognized by Rpi-vnt1. Thus, understanding the underlying mechanism of how Rpi-vnt1.1 perceives AVRvnt1 can provide information for rational utilization of this agronomically important resistance gene in crops.

Although it is well known that host–pathogen interactions are heavily influenced by the environment (8), the impact of physical factors on plant immune sensing is largely unknown. Plants have evolved to adapt to varying environmental conditions not only to optimize their growth and development but also to resist biotic and abiotic stressors (9). However, whereas effectively disrupting pathogen invasion is the major role of plant immune systems, it is required to be tightly regulated to prevent unnecessary immune activation (10, 11). One key environmental factor is light, which

Significance

Plant pathogens, such as Irish potato famine agent *Phytophthora infestans*, remain the most significant threats to global food security. Plant disease resistance is often conferred by nucleotide-binding leucine-rich repeat (NLR) proteins, intracellular immune sensors that recognize and eliminate pathogens. However, little is known about how pathogen-activated NLR immunity is influenced by environmental factors such as light. Here, we show that *P. infestans* manipulation of plant chloroplast function triggers a light-dependent immune response. Our results reveal that light-induced alternative promoter selection regulates plant immune recognition of a pathogen virulence factor by an agriculturally important NLR-type receptor protein.

PLANT BIOLOGY

is not only important for photosynthesis and plant growth but also is essential for plant immune responses (12, 13). In accordance with this view, many infection procedures involve incubation of plants in the dark for certain periods for the successful establishment of disease in laboratory conditions (14). Furthermore, accumulating evidence indicates that photoreceptors positively contribute to the activation of defense-related hormonal pathways (13, 15, 16). However, our understanding of the molecular basis of light dependency of the plant immune system remains mostly obscure. In particular, the extent to which light is required for immune recognition by NLRs and the subsequent execution of defense-related tasks leading to pathogen elimination are poorly understood.

Results

Rpi-vnt1.1–Mediated Disease Resistance to *P. infestans* Is Light-Dependent. To determine the extent to which light regulates NLR-mediated immunity, we used the solanaceous model plant *Nicotiana benthamiana* to screen the light dependency of a set of NLRs against the Irish potato famine pathogen, *P. infestans* (17). We conducted the HR screen by transiently expressing six NLRs and their corresponding *P. infestans* effectors (18) in plants that are either kept under 24 h dark (DD hereafter) or 12 h light/dark (LD hereafter) conditions for 4 d. Remarkably, among the NLR tested, a robust reduction of the HR was observed only for AVRvnt1-triggered activation of Rpi-vnt1.1 (Fig. 1*A* and *SI Appendix*, Fig. S1). Consistent with the HR assays, leaves expressing *Rpi-vnt1.1* provided pathogen resistance only under LD conditions, whereas the control NLR gene *Rpi-blb2* was fully functional regardless of the light (*SI Appendix*, Fig. S2). We further reproduced this phenotype in stable transgenic potato carrying either *Rpi-vnt1.1* (Desiree^Rpi-vnt1.1) or *R3b* (Desiree^R3b). Although both Desiree^Rpi-vnt1.1 and Desiree^R3b plants were fully resistant in LD condition, Desiree^Rpi-vnt1.1 but not Desiree^R3b exposed to DD condition were susceptible to infection (Fig. 1*B*) with typical disease symptoms including sporulation (*SI Appendix*, Fig. S3*A*). We further validated these results, using *P. infestans* isolates P13527 (*AVRvnt1*) and P13626 (*avrvnt1*). As anticipated, P13527 was fully virulent on Desiree^Rpi-vnt1.1 potato plants in DD but not LD conditions, whereas P13626 showed infection symptoms regardless of the light condition tested (*SI Appendix*, Fig. S3*B*). Collectively, these results demonstrate that Rpi-vnt1.1–mediated disease resistance is light-dependent.

Nuclear-Encoded Chloroplast Protein Glycerate Kinase Is Required for AVRvnt1/Rpi-vnt1.1–Mediated Plant Immunity. We next dissected the molecular mechanism underpinning light dependency of Rpi-vnt1.1. We identified the host targets of AVRvnt1 that may be implicated in activation of Rpi-vnt1.1. Yeast two-hybrid (Y2H) screen identified six candidate interactors of AVRvnt1 (*SI Appendix*, Table S1). Validation of yeast two-hybrid assays with full-length host proteins confirmed the interaction between AVRvnt1 and the tomato glycerate 3-kinase (GLYK), a nuclear-encoded chloroplast protein with an N-terminal chloroplast transit peptide (cTP) followed by highly conserved kinase domains (*SI Appendix*, Fig. S4). Furthermore, down-regulation of *GLYK* yielded a robust loss of AVRvnt1/Rpi-vnt1.1–mediated HR (Fig. 2*A* and *SI Appendix*, Fig. S5). GLYK appeared to be specifically required for Rpi-vnt1.1–mediated HR, as GLYK depletion did not perturb HR induced by other NLRs such as R3a and Rpi-blb2 (*SI Appendix*, Fig. S6). Intriguingly, although GLYKs from solanaceous plants including potato, tomato, and *N. benthamiana* interacted with AVRvnt1, *Arabidopsis* GLYK (AtGLYK) failed to associate with AVRvnt1 (*SI Appendix*, Fig. S7*A*). GLYK cTP is strikingly divergent in *Arabidopsis* (*SI Appendix*, Fig. S7*B*), which could account for the loss of AVRvnt1 binding. To test this, we generated a potato GLYK chimera (StGLYK^AtcTP) carrying cTP of the *Arabidopsis* GLYK (*SI Appendix*, Fig. S8*A*).
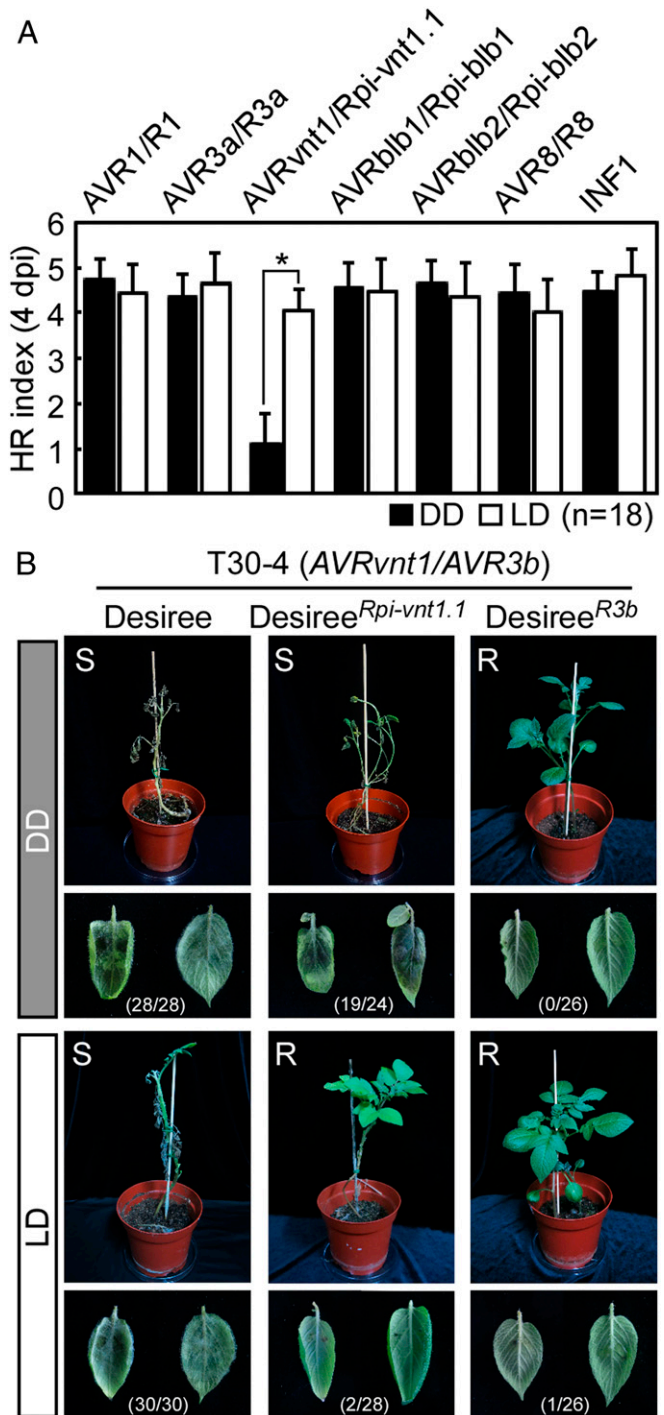

Fig. 1. AVRvnt1/Rpi-vnt1.1–mediated HR and plant immunity is light-dependent. (*A*) HR under DD (24 h dark) and LD (12 h light/12 h dark) conditions. HR phenotypes were scored by HR index analysis (0–5) at 4 d post infiltration (dpi). Bars represent mean SEs of 18 individual infiltration sites from three independent experiments. Asterisk indicates significant differences based on one-way ANOVA (*$P < 0.01$). (*B*) The zoospores of *P. infestans* strain T30-4 were sprayed (*Top*) or dripped (*Bottom*) on Desiree, Desiree^Rpi-vnt1.1, and Desiree^R3b transgenic potato plant in DD and LD conditions. The infected plant and leaves were photographed and counted at 7 d post inoculation. Numbers represent the frequency of infected sites compared to all of the inoculated sites from three independent experiments. S, susceptible; R, resistant.
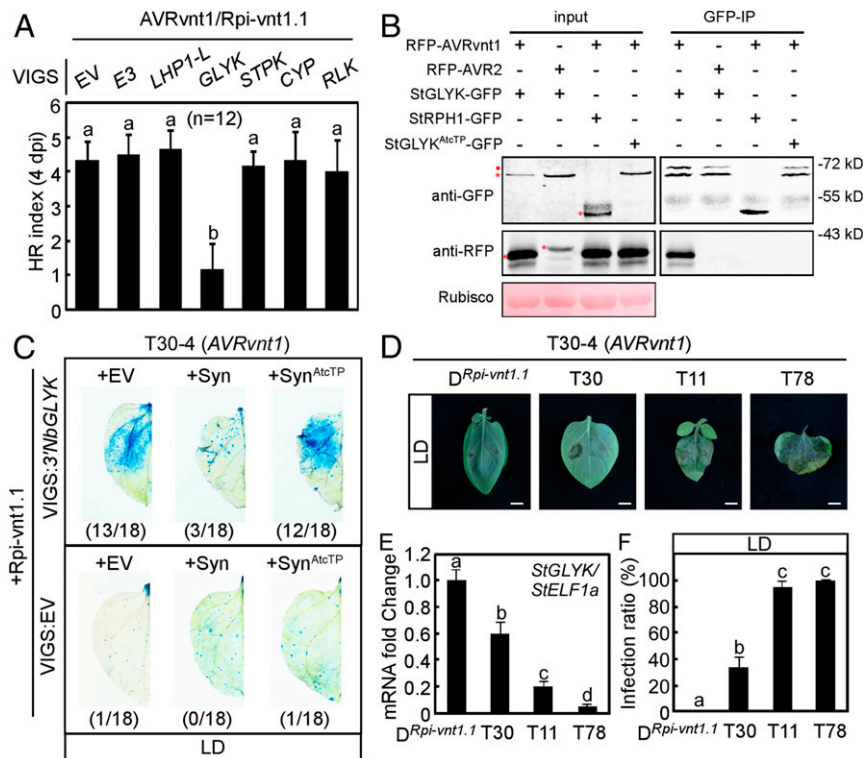
Fig. 2. GLYK is the target of AVRvnt1 required by Rpi-vnt1.1. (*A*) VIGS screen of candidate AVRvnt1 interactors for Rpi-vnt1.1–triggered HR. Phenotypes were scored at 4 dpi. Bars represent mean SEs of 12 individual infiltration sites (*n* = 12) from three independent experiments. (*B*) In vivo coimmunoprecipitation (Co-IP) assay showing AVRvnt1-GLYK interaction. AVR2 (effector protein) and StRPH1 (chloroplast protein) are used as negative controls. The processed and uncleaved GLYK proteins are indicated by red asterisk and red dot, respectively. (*C*) Complementation of Rpi-vnt1.1 function caused by *GLYK* silencing in *N. benthamiana* via synthetic GLYK construct (Syn). Vector control (EV) and Syn^AtcTP are negative controls. Leaves were stained by trypan blue and photographed at 7 dpi. Numbers represent the frequency of infected sites compared to all of the inoculated sites from three biological experiments. (*D*) Disease symptoms of *P. infestans* T30-4 on *StGLYK*-silenced potato lines carrying Rpi-vnt1.1 under LD light condition. Images are obtained at 7 dpi. (Scale bar, 5 mm.) (*E*) The relative *StGLYK/StELF1a* mRNA levels of potato leaves. Values and error bars represent means and SD from three independent experiments, respectively. (*F*) Infection ratio of the potato leaves in *D*. Values represent the percentage of infected sites compared to all of the inoculated sites from three independent experiments. D^Rpi-vnt1.1, Desiree^Rpi-vnt1.1. Different letters correspond to significant differences based on one-way ANOVA (*P* < 0.01, *n* = 24).

The chimeric StGLYK^AtcTP fused to green fluorescent protein (GFP) was able to target chloroplasts in *N. benthamiana* in a similar fashion to wild-type StGLYK (*SI Appendix*, Fig. S8*B*). However, StGLYK^AtcTP failed to interact with AVRvnt1 in planta (Fig. 2*B*) as well as in our Y2H and in vitro protein binding assays (*SI Appendix*, Fig. S9). We therefore conclude that GLYK is a host interactor of AVRvnt1 that is required for activation of Rpi-vnt1.1 and that the N-terminal transit peptide of *Solanaceous* GLYK is essential for AVRvnt1 binding.

To ascertain the function of GLYK in Rpi-vnt1.1–mediated immunity, we generated silencing-resilient *GLYK* constructs to complement GLYK knockdown. These synthetic constructs with shuffled synonymous codons included full-length StGLYK (Syn), StGLYK chimera with AtGLYK's cTP (Syn^AtcTP), and GLYK kinase mutant (Syn^K222R) (*SI Appendix*, Fig. S10 *A* and *B*). We confirmed that Syn, Syn^AtcTP, and Syn^K222R are expressed in *GLYK* knocked down plants, without displaying any autoimmunity (*SI Appendix*, Fig. S10 *C* and *D*). Remarkably, the compromised resistance, and HR phenotypes caused by *GLYK* depletion were rescued by expression of Syn and Syn^K222R but not Syn^AtcTP (Fig. 2*C* and *SI Appendix*, Fig. S10 *E* and *F*). These results indicate that the transit peptide rather than the kinase activity of GLYK is required for recognition of AVRvnt1 by Rpi-vnt1.1. To determine the extent to which GLYK is required for Rpi-vnt1.1–mediated resistance in potato, we stably transformed in the Desiree^Rpi-vnt1.1 with a hairpin-silencing construct targeting potato GLYK (*SI Appendix*, Fig. S5*E*). All three independent

GLYK-silenced Desiree^Rpi-vnt1.1 lines showed enhanced *P. infestans* infection rate that correlated with the *GLYK*-silencing efficiency under LD light condition (Fig. 2 *D–F*). Whereas all of the *GLYK*-silenced Desiree^Rpi-vnt1.1 lines showed equal susceptibility to *P. infestans* under DD light condition (*SI Appendix*, Fig. S5*F*). These data reveal that *GLYK* is essential for AVRvnt1/Rpi-vnt1.1–triggered immunity.

Light Changes Result in APS at *GLYK* Locus and Thus Affect Rpi-vnt1.1–Mediated Immunity. In *Arabidopsis*, *GLYK* produces two varying transcripts through alternative promoter selection (APS) in response to light changes (19). Therefore, we reasoned that light-regulated APS of *GLYK* could account for light dependency of Rpi-vnt1.1. We found light-controlled APS of *GLYK* also occurs in potato. The full-length potato *GLYK* (*StGLYK^FL*) predominantly accumulated in LD condition, whereas *GLYK^FL* transcripts were reduced upon continuous dark exposure. In contrast, the truncated *GLYK* isoform (*StGLYK^cyt*) is up-regulated in DD condition (Fig. 3 *A* and *B* and *SI Appendix*, Fig. S11 *A* and *B*). Also, *GLYK^FL/GLYK^cyt* ratio did not change in plants grown in LD period, and we did not detect any reduction of *Rpi-vnt1.1* messenger RNA (mRNA) in DD condition (*SI Appendix*, Fig. S11 *C* and *D*). Furthermore, we found that *GLYK^FL/GLYK^cyt* ratio changes in outdoor growth conditions, suggesting the APS of *StGLYK* is at play under natural circumstances (*SI Appendix*, Fig. S11*E*).
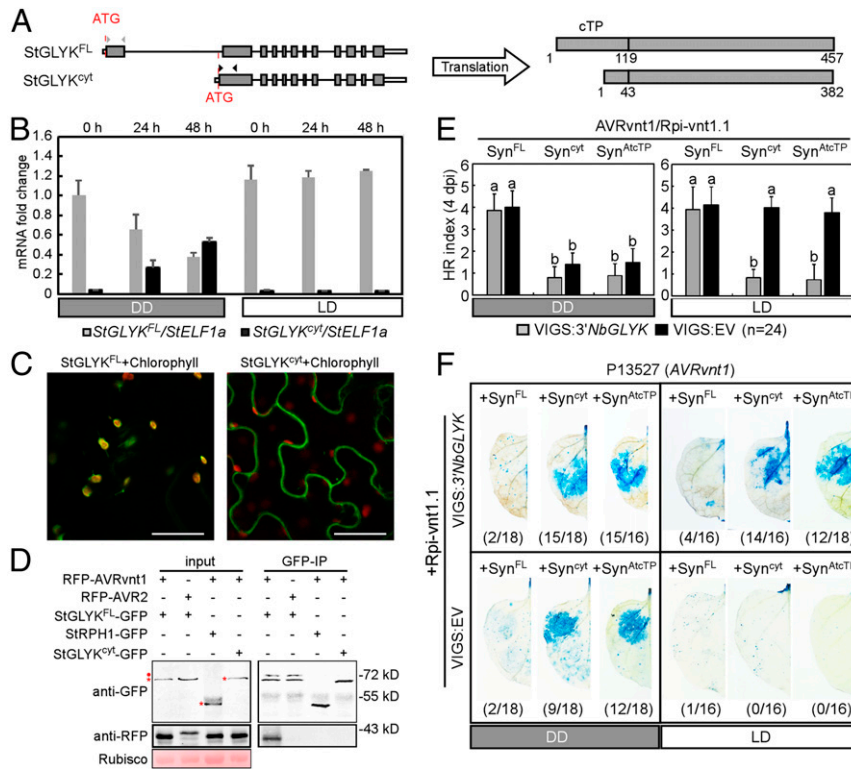
Fig. 3. Rpi-vnt1.1–mediated immunity relies on light-regulated production of potato GLYK isoforms. (*A*) The schematic illustration of APS of *GLYK*. StGLYK[FL] and StGLYK[cyt] pre-mRNA or predicted amino acid sequences are shown. The specific primers to amplify StGLYK[FL] and StGLYK[cyt] transcripts are indicated by gray and black arrowheads, respectively. (*B*) Relative StGLYK[FL]/StELF1a (gray) and StGLYK[cyt]/StELF1a (black) mRNA level of potato leaves under DD or LD light treatment. The RNA samples were collected at 1900 hours in both DD and LD experiments. Values and error bars represent means and SD from three independent experiments, respectively. (*C*) Subcellular localization of StGLYK[FL]-GFP and StGLYK[cyt]-GFP in *N. benthamiana*. Confocal images were obtained at 2 dpi. (Scale bars, 30 μm.) (*D*) In vivo Co-IP assay of GLYK isoforms and AVRvnt1. The processed and uncleaved GLYK protein is indicated by red asterisk and red dot, respectively. (*E*) Rpi-vnt1.1 HR complementation assays using synthetic GLYK isoforms. Syn[AtcTP] chimera is used as negative control. The HR were scored at 4 dpi from three independent experiments. Different letters correspond to significant differences based on one-way ANOVA ($P < 0.01$; $n = 24$). (*F*) Infection complementation assay for loss of Rpi-vnt1.1 function upon GLYK depletion through VIGS. *P. infestans* P13527 (*AVRvnt1*) is used for infection assays. Images were obtained and scored at 7 dpi. Numbers represent the frequency of infected sites compared to all of the inoculated sites from three independent experiments.

These results prompted us to test the extent to which the reduction of *GLYK[FL]* upon exposure to DD accounts for light dependency of Rpi-vnt1.1. We assayed AVRvnt1 association with different GLYK isoforms StGLYK[FL] and StGLYK[cyt] that accumulate in chloroplasts and cytoplasm, respectively (Fig. 3*C* and *SI Appendix*, Fig. S12*A*). Notably, in all protein–protein interaction assays, StGLYK[FL] but not StGLYK[cyt] interacted with AVRvnt1 (Fig. 3*D* and *SI Appendix*, Fig. S12 *B* and *C*), indicating that AVRvnt1 only targets the chloroplast-targeted isoform of GLYK. We then functionally tested the two GLYK isoforms using silencing-resilient synthetic *GLYK* constructs. Consistent with AVRvnt1 binding assays, only Syn[FL] but not Syn[cyt] or Syn[AtcTP] restored Rpi-vnt1.1–mediated HR in *NbGLYK*-silenced plants (Fig. 3*E* and *SI Appendix*, Fig. S13 *A* and *B*). Subsequently, we checked the functions of the two StGLYK isoforms in Rpi-vnt1.1–mediated disease resistance. In *GLYK*-silenced background, only Syn[FL], but not Syn[cyt] and Syn[AtcTP], restored Rpi-vnt1.1–mediated resistance to *P. infestans* strain P13527 (*AVRvnt1*) regardless of the light conditions (Fig. 3*F*). Besides, expression of Syn[FL], Syn[AtcTP], Syn[cyt], or Syn[K222R] did not restore Rpi-vnt1.1–mediated resistance to P13626 (*avrvnt1*) (*SI Appendix*, Fig. S13*C*), indicating that ectopic expression of these *GLYK* constructs does not lead to autoactivation of Rpi-vnt1.1 in *N. benthamiana*. However, in *GLYK*-silenced background, we noted that overexpression of Syn[FL] or Syn[AtcTP] reduced disease symptoms of P13626 (*avrvnt1*) when compared to

control or overexpression of Syn[K222R], whereas this effect was milder with Syn[cyt]. These results suggest that GLYK contributes to basal plant immunity in a kinase activity-dependent manner (*SI Appendix*, Fig. S13 *C* and *D*). The observation that Syn[cyt] partially rescues defense against *P. infestans* indicates that GLYK can still contribute to basal immunity even outside the chloroplasts (19).

GLYK Is a Positive Immune Regulator Destabilized by AVRvnt1. To further explore the potential role of GLYK in basal immunity, we performed infection assays following *GLYK* knockdown in the absence of Rpi-vnt1.1 or in interactions where this resistance gene is ineffective. In multiple independent assays, *NbGLYK*-silenced *N. benthamiana* leaves showed enhanced disease susceptibility compared to control leaves (Fig. 4*A*). Consistently, *StGLYK* knocked down Desiree[Rpi-vnt1.1] were more susceptible to P13626 (*avrvnt1*) (Fig. 4*B*). Thus, our data shows that GLYK contributes to basal immunity in both *N. benthamiana* and potato. To determine whether GLYK function is modulated by AVRvnt1, we coexpressed AVRvnt1 with StGLYK variants and monitored their subcellular distribution. In the presence of AVRvnt1, we observed a substantial reduction of the chloroplastic signal produced by StGLYK but not StGLYK[AtcTP] (Fig. 4*C*). We further confirmed these results through tissue fractionation and Western blotting, revealing that AVRvnt1 impairs accumulation of StGLYK in both total and chloroplast
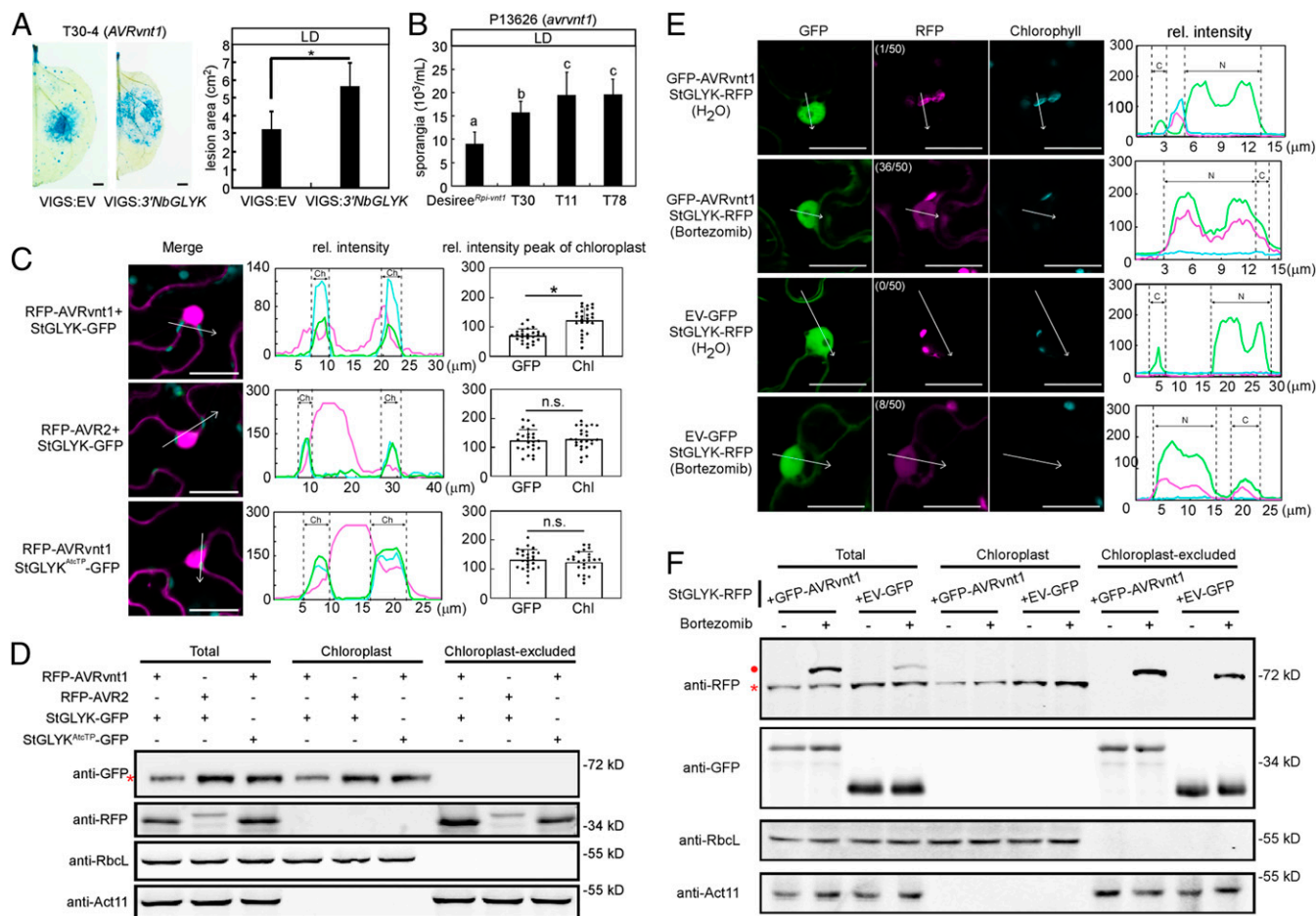
Fig. 4. AVRvnt1 prevents GLYK accumulation in chloroplasts to subvert GLYK's positive role in immunity. (*A*) *NbGLYK*-silenced plant is more susceptible to *P. infestans*. Leaves from *NbGLYK*-silenced and control *N. benthamiana* plant were inoculated with zoospores of T30-4 in LD light condition. The results were photographed and measured at 7 dpi from three independent experiments (*$P < 0.01$; one-way ANOVA, $n = 24$). (Scale bar, 50 mm.) (*B*) *StGLYK*-silenced plants generate more sporangia after *P. infestans* infection. Leaves from *StGLYK*-silenced and control Desiree$^{Rpi-vnt1.1}$ potato plant were inoculated with zoospores of P13626 in LD light condition. Sporangia recovered from infected leaves were counted at 10 dpi from three independent experiments. Different letters correspond to significant differences based on one-way ANOVA ($P < 0.01$, $n = 12$). (*C*) The impact of AVRvnt1 on subcellular distribution of GLYK. Both proteins with different fluorescent tags were expressed in *N. benthamiana* by agroinfiltration for 2 d. The fluorescence images (*Left*) were obtained by confocal microscope. Relative fluorescent intensities of the constructs were measured across the white arrows crossing the chloroplasts (*Middle*) using the ZEN software. Ch represents chloroplast. Statistic bar graphs (*Right*) showing relative fluorescence of multiple chloroplasts from three independent experiments (Chl represents ChloropylI. *$P < 0.01$; n.s., no significance; one-way ANOVA, $n = 25$). (Scale bar, 30 μm.) (*D* and *F*) GLYK proteins from separated fractions detected by Western blot. The proteins expressed in *N. benthamiana* were extracted from total, chloroplast fraction and chloroplast-excluded fraction and detected by Western blot. The predicted processed and uncleaved GLYK proteins are indicated by red asterisk and red dot, respectively. The anti-RbcL and anti-Act11 were controls of isolated fractions. (*E*) Fluorescent measurements of AVRvnt1 and GLYK following proteasome inhibition. Both proteins were expressed in *N. benthamiana* by agroinfiltration. Bortezomib (100 μM) or H$_2$O were infiltrated 6 h before microscopy observation (*Left*). Numbers represent the frequency of cells showing GLYK cytoplasmic localization compared to 50 calculated cells from three biological experiments. Two days after agro-infiltration, relative fluorescence signals produced by the GFP/RFP constructs as well as the chloroplast autofluorescence were measured throughout the arrows that cross the chloroplasts (*Right*) using the ZEN software. "C" represents cytoplasm, and "N" represents nuclear. (Scale bar, 25 μm.)

fractions (Fig. 4*D*). We further verified these observations during *P. infestans* infection (*SI Appendix*, Fig. S14 *A* and *B*). Meanwhile, we also found that ectopic expression of StGLYK^{AtcTP} confers more resistance than expression of full-length StGLYK to *P. infestans* carrying AVRvnt1(*SI Appendix*, Fig. S14*C*). Based on these results, we reasoned that AVRvnt1 intercepts GLYK's trafficking to chloroplasts and potentially promotes GLYK depletion via the proteasome. To test this idea, we coexpressed StGLYK with AVRvnt1 in the presence or absence of the proteasome inhibitor bortezomib (20). Remarkably, upon proteasome inhibition, we noted a substantial overlap of AVRvnt1 and GLYK fluorescence signals in the cytoplasm and nucleus (Fig. 4*E*). Consistent with these results, we detected enhanced protein levels of GLYK isoform carrying the transit peptide in

total extracts following proteasome inhibition (Fig. 4*F*). In line with the hypothesis that AVRvnt1 intercepts GLYK trafficking to chloroplasts, this effect was substantially stronger in the presence of GFP-AVRvnt1 compared to GFP control in both total and chloroplast free extracts. Following proteasome inhibition, we also noted a slight increase in the noncleaved GLYK protein in the absence of AVRvnt1, suggesting that proteasome regulates GLYK levels by targeting the full-length GLYK, and AVRvnt1 further enhances this endogenous process (Fig. 4*F*).

Discussion

Light-dependent APS regulates photorespiration (19, 21), but an immune regulatory role of APS in NLR functioning is previously unknown. We report an unprecedented light-dependent immune

mechanism in which light-induced APS determines functioning of the agronomically important NLR protein Rpi-vnt1.1. We found that the activation of Rpi-vnt1.1 requires the nuclear-encoded GLYK isoform localized to chloroplasts, which is targeted by AVRvnt1. Rpi-vnt1.1 can indirectly sense AVRvnt1 only in the presence of light, as light-induced APS leads to the production of GLYK transcripts that carry an intact chloroplast transit signal which is required for AVRvnt1 binding. We also uncovered an immune function of GLYK in contributing to defense against *P. infestans* and a pathogen counterstrategy that prevents GLYK's trafficking to chloroplasts.

Our results support a model where the *P. infestans* effector AVRvnt1 promotes proteasome-mediated degradation of the chloroplast-targeted GLYK isoform, thereby subverting GLYK's positive role in immunity (Fig. 4). We propose that Rpi-vnt1.1 monitors GLYK's trafficking to chloroplasts, resulting in Rpi-vnt1.1 activation when this process is interrupted by AVRvnt1. However, down-regulation of GLYK compromises AVRvnt1-triggered activation of Rpi-vnt1.1 (Fig. 2), suggesting that interaction between AVRvnt1 and GLYK is necessary for Rpi-vnt1.1–mediated immunity. Rpi-vnt1.1 may either sense the AVRvnt1–GLYK complex or potential conformational changes in GLYK structure stimulated by AVRvnt1. Whether Rpi-vnt1.1 physically interacts with GLYK or the GLYK-AVRvnt1 complex remains unclear. We could not address these possibilities because both N- and C-terminal epitope tagging of Rpi-vnt1.1 resulted in impaired Rpi-vnt1.1 function. Alternatively, Rpi-vnt1.1 could sense GLYK peptides (N-terminal chloroplast transit peptide) that are released by the proteasome, a process which is stimulated by AVRvnt1. Nevertheless, Rpi-vnt1.1 appears to safeguard chloroplast functions remotely by detecting perturbations in transport of a chloroplast cargo targeted by *P. infestans*. Determining the subcellular localization of Rpi-vnt1.1 is required to reach definitive conclusions.

Interestingly, Rpi-vnt1.1 is the homolog of tomato Tm-2^2 which requires chloroplast protein NbRbCS to mediate resistance to tomato tobamovirus (6, 22). These findings further support the emerging roles of chloroplasts in plant immunity and are in line with the recent discoveries which revealed that pathogens deploy effectors to perturb chloroplast functions (23–27). Down-regulation of GLYK in *N. benthamiana* enhances plant susceptibility to *P. infestans* (Fig. 4 *A* and *B*) indicating that GLYK could be the operative virulence target of AVRvnt1. In the presence of light, AVRvnt1 could promote the depletion of GLYK to interfere with energy production in chloroplasts which can be used to synthesize defense-related compounds. Alternatively, AVRvnt1 could prevent redox toxicity caused by altered GLYK function in the chloroplasts stimulated by the pathogen attack in the presence of light. To date, there is no report of a *P. infestans* effector that localizes to the chloroplasts. However, our results indicate that this may not be necessary as *P. infestans* can remotely subvert chloroplast functions by controlling the transport of nuclear-encoded chloroplast proteins (Fig. 4 *C*–*F*). Our findings provide a mechanistic understanding of the impact of light on NLR-triggered plant immunity and strategies employed by the pathogens to subvert defense-related chloroplast functions.

Materials and Methods

Plasmid Construction. All primers used for cloning and experiments are listed in *SI Appendix*, Table S2. All plasmids constructed in this study are listed in *SI Appendix*, Table S3. All of the templates used for PCR amplification come from genomic DNA (gDNA) or complementary DNA (cDNA) of *P. infestans* (strain T30-4), *N. benthamiana*, *Solanum tuberosum* (Desiree cultivar), *Solanum lycopersicum* (Heinz), *Arabidopsis* (Columbia), or from plasmids in published study (18). Enzymes from Vazyme (Cat No. P515 01/02/03) and Takara (Cat No. R001A) are used for PCR amplification and verification. Enzymes from Takara (Cat No. 1010S, 1040S, 1042S, 1094S, 2011A) and Vazyme (Cat No. C115-01/02) are used for nucleic acid digestion and ligation.

Growth Condition of Plant Material and Microbial Strains. *S. tuberosum* aseptic seedlings were grown on Murashige and Skoog (MS) medium in growth chamber under 16 h light (100–150 μmol m^{-2} s^{-2})/8 h dark cycle, temperature 20–24 °C, relative humidity 60%. After 2 wk growth, the medium was carefully removed, and the seedlings were transferred and grown in sterilized soil before the experiments. For outdoor growth, plants were grown in pots under ~11 h day/~13 h night, with the location at 32°2′6″ N, 118°50′23″ W and temperature from 2 to 10 °C. *N. benthamiana* seeds were germinated and grown in growth chamber under the same condition before the experiments. The LD and DD conditions only change the time period of the light treatment. *P. infestans* strains T30-4, P13626, P13527, and 88069td (28) were grown on the rye sucrose agar (RSA) with 10% V8 vegetable juice medium plate at 18 °C. *Escherichia coli* strains DH5α, JM109, and BL21 and *Agrobacterium tumefaciens* strain GV3101 were grown on the Luria-Bertani (LB) medium plate at 37 °C and 30 °C, respectively.

P. infestans Infection Assays. *P. infestans* strains were grown on RSA+V8 medium plate at 18 °C for 14 d. The sporangia were scraped into cold, distilled water and incubated at 4 °C for about 2 h until zoospore release. The zoospore suspension was collected at a concentration of 14,000 sporangia/mL before inoculation. The whole-plant and detached leaves infection assays were reported (29). The zoospore suspension was sprayed or dropped on the plant leaves and incubated in a controlled environment cabinet at 18 °C, relative humidity 95–100%; lesions were scored at 7 dpi. The sporangia on the infected leaves were photographed by microscope and were counted after being vortexed in 5 mL H$_2$O at 10 dpi. The infected *N. benthamiana* leaves were stained by trypan blue as previously described (30). Leaves were soaked into trypan blue solution (10 mL 85% lactic acid aqueous, 10 mL water-saturated phenol, 10 mL 98% glycerol, 10 mL distilled water, 15 mg trypan blue) overnight. Stained leaves were then transferred into ethanol and incubated at 37 °C for 24 h before observation. Numbers at the bottom of the leaf image represent the frequency of successfully infected sites compared to all inoculated sites from three independent experiments.

Agrobacterium Transient Assay and HR Assays. Gene transient expressions in *N. benthamiana* were performed as previously described (31). Gene sequence cloned for expression were driven by 35S promoter, except Rpi-vnt1.1 driven by *Rpi-blb3* gene promoter. Agrobacterium-containing expression constructs were grown in LB medium and resuspended by infiltration buffer (10 mM MgCl$_2$, 10 mM 2-[*N*-morpholino] ethanesulfonic acid pH = 5.6, 200 μM acetosyringone). The optical densities at 600 nm (OD600) of cell suspensions were used as follows: AVRvnt1/Rpi-vnt1.1 = 0.1/0.2, AVR1/R1 = 0.2/0.2, AVR3a/R3a = 0.2/0.2, AVRblb1/Rpi-blb1 = 0.2/0.2, AVRblb2/Rpi-blb2 = 0.2/0.2, AVR8/R8 = 0.2/0.2, INF1 = 0.2, and the OD600 of all of the other proteins' expressions were 0.4. Four-week-old *N. benthamiana* leaves were chosen for infiltration. *P. infestans* effector protein AVR2 (PITG_22870) and *S. tuberosum* chloroplast protein StRPH1 (PGSC0003DMT400060330) showed similar subcellular localization with AVRvnt1 (PITG_16294) and StGLYK (PGSC0003DMT400006578), respectively, are used as a negative controls (25, 32). Western blot and confocal observation were performed at 2 dpi. The HR were scored at 4 dpi and were classified as six types. All of the experiments contain three independent replicates, and the number (*n*) of infiltrated sites were shown.

Yeast-Two-Hybrid Assays. Y2H interaction screening was performed as previously described (33). *AVRvnt1* and *AVR2* without signal peptide and RxLR motif (-SP-RxLR) were cloned into yeast expression construct pGBKT7, tomato cDNA library, and the candidate genes (*SI Appendix*, Table S1) including *AtGLYK* (AT1G80380) were cloned into pGADT7. Each pair of constructs were cotransformed into yeast strain AH109 and were selected using SD-Trp-Leu medium and SD-Trp-Leu-His-Ade medium with X-α-gal (80 mg/L) at 30 °C for 5 d. Experiments were repeated three times with similar results.

Confocal Microscopy. Confocal microscopy observation was performed on the *N. benthamiana* leaf patches 2 d post infiltration by LSM 710 laser-scanning microscope with 20×/0.8 or ×40/0.95 objective lens (Carl Zeiss). The GFP, red fluorescent protein (RFP), and autofluorescence were scanned under excitation of 488- and 514-nm laser with emissions collected between 535 and 636 nm. The conditions for microscopy data acquisition were consistent across samples. The images were processed by ZEISS ZEN Microscope Software and Adobe Photoshop at the same time.

Gene Silencing and Complementation Assays. Virus-induced gene silencing (VIGS) was performed in *N. benthamiana* as described (34). The specific DNA fragments with 300 base pairs (bp) from *E3* (Niben101Scf00868g03005.1), *LHP1-L* (Niben101Scf00215g06004.1), *GLYK* (Niben101Scf18107g00014.1), *STPK* (Niben101Scf00850g01028.1), *CYP* (Niben101Scf02763g05012.1), and *RLK* (Niben101Scf08873g01009.1) predicted by VIGS tool (https://vigs.solgenomics.net/) were cloned into Tobacco Rattle Virus (TRV) RNA2 (pYL279) construct (*SI Appendix*, Table S1). *A. tumefaciens* strain GV3101 carry TRV2 and TRV RNA1 (pYL155) constructs were mixed in a 1:1 ratio and infiltrated into 2-wk-old *N. benthamiana* leaves. Two weeks post infiltration, upper leaves were used for the experiments. For hairpin RNA interference (RNAi), the chalcone synthase (*CHSA*) intron was amplified from plasmid pFGC5941. The PCR-amplified *3'StGLYK* cDNA fragments were overlapped to the 5' and 3' end of *CHSA* intron from two directions. The overlapped fragment was inserted in p1300 vector and transformed into agrobacterium strain GV3101 before potato transformation which was done by Wuhan Double-helix Biology Science and Technology Company. For the complementation assays, the shuffled synonymous synthetic *StGLYK* sequences were generated by Genscript and cloned into expression constructs pICH86988 with C-terminal GFP tag. Synthetic proteins were coexpressed with AVRvnt1/Rpi-vnt1.1 during HR test assays.

In Vitro Pull-Down, In Vivo Coimmunoprecipitation, and Western Blot Assays. For the in vitro pull-down assays, genes were cloned in pGEX-4T-2 (GST tag) and pET32a (His tag) constructs, respectively. Proteins were expressed in *E. coli* strain BL21 and extracted as previously described. Proteins with GST tag were incubated with glutathione agarose beads (Thermo Fisher Scientific, 16101) at 4 °C for 4 h and washed by wash buffer (50 mM NaCl, 50 mM Tris·HCl pH = 7.5, 0.05% Tritonx100) three times. Then, proteins with His tag were incubated with the beads at 4 °C for 4 h. Finally, the beads were washed three times and detected by anti-GST (1:2,000, Abmart, M20007) and anti-His antibodies (1:2,000, Abmart, M20001) by Western blot. For the in vivo coimmunoprecipitation assays, proteins were expressed in *N. benthamiana* and extracted by the PH-increased lysis buffer (150 mM NaCl, 10 mM Tris·HCl pH = 8.3, 0.5 mM ethylenediaminetetraacetic acid [EDTA], 1% Tritonx100) with 1% protease inhibitor mixture (Sigma-Aldrich, P9599). The total proteins were incubated with GFP-Trap_A beads (Chromotek, ACT-CM-GFA0050) at 4 °C for 2 h and washed by washing buffer (150 mM NaCl, 10 mM Tris·HCl pH = 7.5, 0.5 mM EDTA, 1% protease inhibitor mixture) three times. Proteins were detected by anti-GFP (1:2,000, Abmart, P30010) and anti-RFP (1:2,000, Chromotek, 6G6) antibodies. All of the experiments were repeated three times with similar results.

RACE and qRT-PCR Analysis. For each sample, total RNA was extracted by Total RNA Kit (OMEGA, R6934-01); 1 μg RNA was used for reverse transcription to generate cDNA by kit (Vazyme, R101). Rapid amplification of cDNA ends (5'RACE) analysis was performed using kit (Thermo Fisher Scientific, 18374058)

according to the manufacturer's instructions. qRT-qPCR was performed to detect gene relative expression, *N. benthamiana NbELF1a* (Niben101Scf34389g00002.1) and potato *StELF1a* (PGSC0003DMT400059830) were used as reference genes, respectively. In total, 20 μL qPCR reaction mixture (Vazyme, Q221) containing 2 μL cDNA was processed by ABI Prism 7500 Fast Real-Time PCR system and results contain three biological replicates. The results were calculated by ABI 7500 System Sequence Detection Software. Values and error bars of all the column diagrams in this article represent means and SD from three independent experiments, respectively. Two GLYK isoform sequences generated by 5'RACE experiments were submitted to National Center for Biotechnology Information, "BankIt2308282 GLYK-1 MT002831" for full-length isoform and "BankIt2308282 GLYK-2 MT002832" for cytoplasmic isoform.

Plant Fraction Separation. *N. benthamiana* leaf chloroplast and chloroplast-excluded fraction were separated as described (35). Leaves weighing 0.1 g were homogenized in 400 μL ice-cold isolation buffer (0.33 M Sorbitol, 50 mM Hepes pH = 7.0, 0.1% bovine serum albumin [BSA], 2 mM EDTA, 1 mM $MgCl_2$) using a precooled glass homogenizer. The homogenate was filtered through a 50-μm mesh filter and kept on ice and in the dark for 5 min. Filtered chloroplast-containing homogenate (400 μL) was placed carefully on top of the 40% Percoll layer and centrifuged at 1,700 *g* at 4 °C for 6 min. The intact chloroplasts will sediment as a green pellet, whereas the chloroplast excluded fraction remains on the top. Chloroplasts were shock-frozen in liquid nitrogen and resuspended in 50 μL of ice-cold protein extraction buffer and centrifuged at 15,000 *g* at 4 °C for 10 min. The supernatant was extracted for Western blot. Anti-RbcL (Beijing Protein Innovation, AbP80037-A-SE) and anti-Act11 (Abmart, M20009) are used to detect chloroplast fraction and chloroplast-excluded fraction, respectively.

Motif Prediction. The chloroplast transit peptides of *GLYK* and *RPH1* were predicted by ChloroP from website (http://www.cbs.dtu.dk/services/ChloroP/).

Data Availability. All data are contained in the manuscript and *SI Appendix*. Two GLYK isoform sequences generated by 5'RACE experiments have been deposited to National Center for Biotechnology Information GenBank, https://www.ncbi.nlm.nih.gov (accession nos. MT002831 and MT002832).

1. J. D. Jones, J. L. Dangl, The plant immune system. *Nature* **444**, 323–329 (2006).
2. W. Wang, B. Feng, J. M. Zhou, D. Tang, Plant immune signaling: Advancing on two frontiers. *J. Integr. Plant Biol.* **62**, 2–24 (2020).
3. J. D. Jones, R. E. Vance, J. L. Dangl, Intracellular innate immune surveillance devices in plants and animals. *Science* **354**, aaf6395 (2016).
4. J. L. Dangl, D. M. Horvath, B. J. Staskawicz, Pivoting the plant immune system from dissection to deployment. *Science* **341**, 746–751 (2013).
5. C. H. Wu, L. Derevnina, S. Kamoun, Receptor networks underpin plant immunity. *Science* **360**, 1300–1301 (2018).
6. S. J. Foster *et al.*, Rpi-vnt1.1, a *Tm-2(2)* homolog from *Solanum venturii*, confers resistance to potato late blight. *Mol. Plant Microbe Interact.* **22**, 589–600 (2009).
7. M. Pais *et al.*, Gene expression polymorphism underpins evasion of host immunity in an asexual lineage of the Irish potato famine pathogen. *BMC Evol. Biol.* **18**, 93–103 (2018).
8. K. B. Scholthof, The disease triangle: Pathogens, the environment and society. *Nat. Rev. Microbiol.* **5**, 152–156 (2007).
9. A. C. Velásquez, C. D. M. Castroverde, S. Y. He, Plant-pathogen warfare under changing climate conditions. *Curr. Biol.* **28**, R619–R634 (2018).
10. Y. T. Cheng, L. Zhang, S. Y. He, Plant-microbe interactions facing environmental challenge. *Cell Host Microbe* **26**, 183–192 (2019).
11. X. F. Xin *et al.*, Bacteria establish an aqueous living space in plants crucial for virulence. *Nature* **539**, 524–529 (2016).
12. J. Chaiwanon, W. Wang, J. Y. Zhu, E. Oh, Z. Y. Wang, Information integration and communication in plant growth regulation. *Cell* **164**, 1257–1268 (2016).
13. C. L. Ballaré, Light regulation of plant defense. *Annu. Rev. Plant Biol.* **65**, 335–363 (2014).
14. H. E. Yigal Cohen, T. Sadon, Light-induced inhibition of sporangial formation of *Phytophthora infestans* on potato leaves. *Can. J. Bot.* **53**, 2680–2686 (1975).
15. J. E. Moreno, Y. Tao, J. Chory, C. L. Ballaré, Ecological modulation of plant defense via phytochrome control of jasmonate sensitivity. *Proc. Natl. Acad. Sci. U.S.A.* **106**, 4935–4940 (2009).
16. P. V. Demkura, G. Abdala, I. T. Baldwin, C. L. Ballaré, Jasmonate-dependent and -independent pathways mediate specific effects of solar ultraviolet B radiation on leaf phenolics and antiherbivore defense. *Plant Physiol.* **152**, 1084–1095 (2010).
17. V. G. Vleeshouwers *et al.*, Understanding and exploiting late blight resistance in the age of effectors. *Annu. Rev. Phytopathol.* **49**, 507–531 (2011).
18. C. H. Wu *et al.*, NLR network mediates immunity to diverse plant pathogens. *Proc. Natl. Acad. Sci. U.S.A.* **114**, 8113–8118 (2017).
19. T. Ushijima *et al.*, Light controls protein localization through phytochrome-mediated alternative promoter selection. *Cell* **171**, 1316–1325 e12 (2017).
20. Q. Ling *et al.*, Ubiquitin-dependent chloroplast-associated protein degradation in plants. *Science* **363**, eaav4467 (2019).
21. K. H. Wrighton, Transcription: Shedding light on alternative promoter selection. *Nat. Rev. Genet.* **19**, 4–5 (2018).
22. J. Zhao *et al.*, The rubisco small subunit is involved in tobamovirus movement and Tm-2²-mediated extreme resistance. *Plant Physiol.* **161**, 374–383 (2013).
23. J. L. Caplan, P. Mamillapalli, T. M. Burch-Smith, K. Czymmek, S. P. Dinesh-Kumar, Chloroplastic protein NRIP1 mediates innate immune receptor recognition of a viral effector. *Cell* **132**, 449–462 (2008).
24. M. de Torres Zabala *et al.*, Chloroplasts play a central role in plant defence and are targeted by pathogen effectors. *Nat. Plants* **1**, 15074 (2015).
25. K. Belhaj, B. Lin, F. Mauch, The chloroplast protein RPH1 plays a role in the immune response of Arabidopsis to *Phytophthora brassicae*. *Plant J.* **58**, 287–298 (2009).

26. M. van Damme et al., Downy mildew resistance in Arabidopsis by mutation of ho-moserine kinase. *Plant Cell* **21**, 2179–2189 (2009).

27. B. Petre et al., Rust fungal effectors mimic host transit peptides to translocate into chloroplasts. *Cell. Microbiol.* **18**, 453–465 (2016).

28. S. C. Whisson et al., A translocation signal for delivery of oomycete effector proteins into host plant cells. *Nature* **450**, 115–118 (2007).

29. P. H. F. H. E. Stewart, D. C. McCalmont, R. L. Wastie, Correlation between glasshouse and field tests for resistance to foliage blight caused by *Phytophthora infestans*. *Potato Res.* **26**, 41–48 (1983).

30. J. L. Peng et al., Harpin-elicited hypersensitive cell death and pathogen re-sistance require the *NDR1* and *EDS1* genes. *Physiol. Mol. Plant Pathol.* **62**, 317–326 (2003).

31. J. I. Bos et al., The C-terminal half of *Phytophthora infestans* RXLR effector AVR3a is sufficient to trigger R3a-mediated hypersensitivity and suppress INF1-induced cell death in *Nicotiana benthamiana*. *Plant J.* **48**, 165–176 (2006).

32. D. G. Saunders et al., Host protein BSL1 associates with *Phytophthora infestans* RXLR effector AVR2 and the *Solanum demissum* immune receptor R2 to mediate disease resistance. *Plant Cell* **24**, 3420–3434 (2012).

33. J. Luban, S. P. Goff, The yeast two-hybrid system for studying protein-protein inter-actions. *Curr. Opin. Biotechnol.* **6**, 59–64 (1995).

34. S. Bachan, S. P. Dinesh-Kumar, Tobacco rattle virus (TRV)-based virus-induced gene silencing. *Methods Mol. Biol.* **894**, 83–92 (2012).

35. J. Klinkenberg, Extraction of chloroplast proteins from transiently transformed *Ni-cotiana benthamiana* leaves. *Bio-Protocol* **4**, e1238 (2014).